Evaporation-Induced Self-Assembly: Functional Nanostructures Made Easy

C. Jeffrey Brinker

Abstract

The following article is an edited transcript based on the MRS Medalist presentation given by C. Jeffrey Brinker (Sandia National Laboratories and the University of New Mexico) on December 3, 2003, at the Materials Research Society Fall Meeting in Boston. Brinker received the Medal for "his pioneering application of principles of sol-gel chemistry to the self-assembly of functional nanoscale materials." Nature combines hard and soft materials, often in hierarchical architectures, to obtain synergistic, optimized properties with proven, complex functionalities. Emulating natural designs in robust engineering materials using efficient processing approaches represents a fundamental challenge to materials chemists. This presentation reviews progress on understanding so-called evaporation-induced silica/surfactant self-assembly (EISA) as a simple, general means of preparing porous thin-film nanostructures. Such porous materials are of interest for membranes, low-dielectric-constant (low-*k*) insulators, and even '"nano-valves" that open and close in response to an external stimulus. EISA can also be used to simultaneously organize hydrophilic and hydrophobic precursors into hybrid nanocomposites that are optically or chemically polymerizable, patternable, or adjustable.

Keywords: *azobenzene, functional materials, nanocomposites, nanocrystals, nanostructures, self-assembly.*

Introduction

It is certainly a great honor to receive the MRS Medal and to have the opportunity to present some of our research to the MRS audience, which includes a great number of good friends and colleagues.

In his MRS Medal lecture, Ivan K. Schuller emphasized that his research incorporated few biological concepts or components (see article by Schuller in this issue of *MRS Bulletin*). In contrast, our research has been largely inspired by biology. From a materials perspective, biology serves as an excellent model. Biological systems are composed of nanoscale components and exhibit complex functionalities that have evolved over millions of years. We look to such natural systems to see if we can emulate some of these proven biological designs and incorporate them into robust engineering materials. Occasionally, we can be so presumptuous as to consider improving upon nature's designs by nanostructuring and using a broader palette of chemicals. We also want to integrate these nanoscale materials into structures that operate on larger length scales that allow electrical, optical, or fluidic addressability and interrogation. This has directed our research largely toward making thin films.

When we look at natural materials, we see that nature often combines multiple hard and soft materials in hierarchical designs to obtain synergistic and often optimized properties or combinations of properties. This is an interesting aspect of biology that we can try to mimic in engineering materials.

In constructing such composite structures, a significant challenge is how to controllably organize or define multiple materials on multiple length scales. To address this challenge, we have combined sol-gel chemistry with molecular self-assembly in several evaporation-driven processing procedures collectively referred to as evaporation-induced self-assembly (EISA).

Self-Assembly Procedures

Self-assembly is defined as the spontaneous, reversible organization of preexisting components by means of non-covalent interactions such as hydrogen bonding and van der Waals, electrostatic, or hydrophobic forces.[1] Although the forces or energies of individual interactions are on the order of kT (k is the Boltzmann constant; T is temperature), the collective behavior of the huge number of these (possibly directional) interactions drives the reliable and reproducible organization of components into assemblies that represent a global or local equilibrium. During the last decade, self-assembly has emerged as a promising approach to defining material features on length scales smaller than those conveniently accessible by lithography. As such, *molecular* self-assembly has remained a very active area of research.

Molecular self-assembly employs molecules that are encoded or programmed by means of surface properties, shape, charge, and so on to organize in specific arrangements without external intervention. Our work uses two-sided molecules called surfactants (commonly known as detergents), composed of hydrophobic and hydrophilic parts.

As understood by detergent phase diagrams (Figure 1), above a critical concentration, surfactants added to water (and, optionally, oil) self-assemble into spherical micelles that maintain their hydrophilic parts in contact with water and shield the hydrophobic parts (along with any oil) within the micellar interior. At higher concentrations, micelles further self-organize into periodic structures called mesophases—true thermodynamically defined phases that obey the Gibbs phase rule.

As recognized by Kresge et al.,[2] surfactant self-assembly conducted in water with added hydrophilic components (e.g., silicic acid or hydrolyzed metal alkoxides)

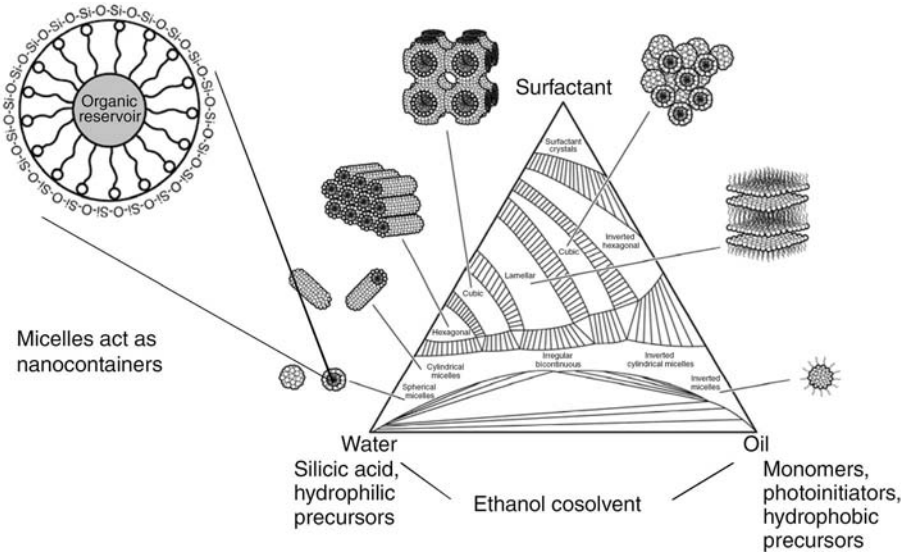

Figure 1. Generic detergent phase diagram (provided by Davis and Scriven, University of Minnesota.)

provides a robust synthetic approach to transcribing the nanoscopic order of a mesophase into inorganic materials. Through electrostatic and hydrogen-bonding interactions, the hydrophilic components organize around the hydrophilic micellar exteriors and condense to form oxides—essentially, fossilized replicas of the mesophases.

Less well recognized is that added hydrophobic components (e.g., organic monomers, initiators, etc.) can be sequestered within the hydrophobic micellar interiors. Surfactant added to water and oil allows the oil to be solubilized within the micelles, making it water-soluble. This is like our everyday experience of washing dishes using household detergent. Simultaneous organization of otherwise immiscible hydrophilic and hydrophobic precursors into mesophases by surfactant self-assembly provides an efficient, viable route to the formation of ordered organic/inorganic nanocomposites.

The first inorganic mesophases were formed hydrothermally as powders, just like zeolites. When I first became aware of the Mobil work[2] on mesoporous silicas, I thought it would be important to make these materials as films, because after calcination to remove the surfactants, they would be useful as membranes, sensors, and low-dielectric-constant (low-*k*) insulators. From my understanding of evaporation-driven sol-gel thin-film deposition,[3] the idea was to dilute the silica/water/surfactant system with ethanol to create a homogeneous solution and then rely on ethanol and water evaporation during dip-coating (or other coating methods) to progressively concentrate surfactant and silica in the depositing film, driving micelle formation and subsequent continuous silica/surfactant mesophase self-assembly.

One of the crucial aspects of this process, in terms of the sol-gel chemistry, is to work under conditions where the condensation rate of the hydrophilic silicic acid precursors [≡Si-OH, where ≡ represents bonds to other hydroxyls (OH) or siloxanes (OSi≡), and Si-OH is referred to as a silanol group] is minimized. The idea is not to frustrate the self-assembly process by gelation that would kinetically trap the system at an intermediate nonequilibrium state. We want the structure to self-assemble, then solidify with the addition of a siloxane condensation catalyst or by heating to form the desired mesoporous product. Operating at an acidic pH (pH = 2) minimizes the condensation rate of silanols to form siloxanes, Si–O–Si.[3] In addition, hydrogen bonding and electrostatic interactions between silanols and hydrophilic surfactant head groups can further reduce the condensation rate. These combined factors maintain the depositing film in a fluid state, even beyond the point where ethanol and water are largely evaporated. This allows the deposited film to be self-healing and enables the use of virtually any evaporation-driven process (spin-coating, inkjet printing, or aerosol proc-

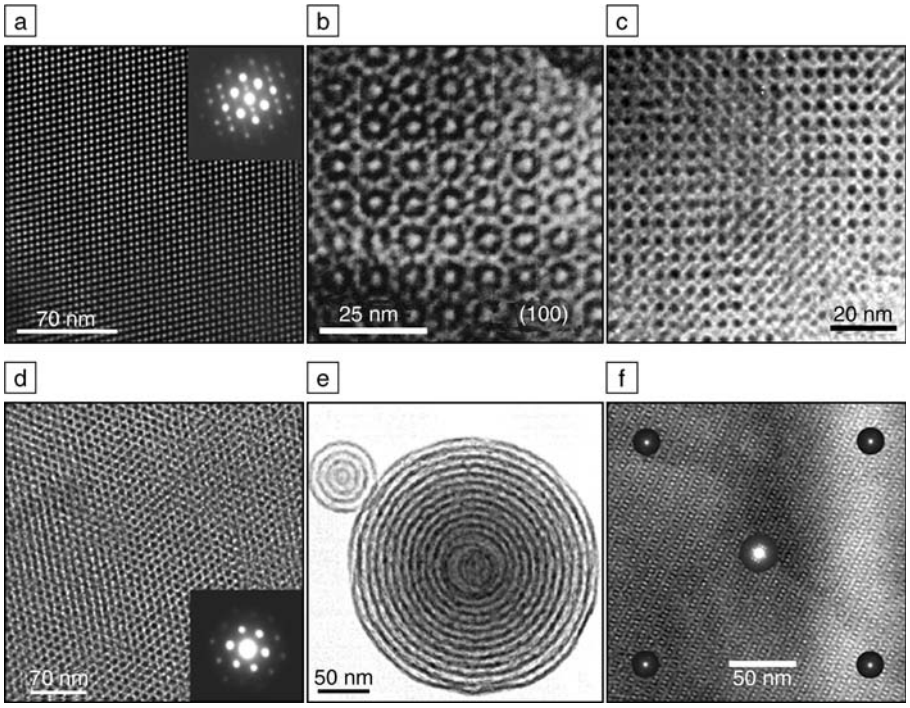

Figure 2. Representative transmission electron microscopy images of self-assembled porous and composite nanostructured coatings[4,8,17] and particles.[7] (a), (b), (d): Porous thin films exhibiting ordered three-dimensional networks of nanopores prepared using the cationic surfactant cetyltrimethylammonium bromide. (c) Three-dimensional nanocrystalline gold/silica cubic array.[17] (e) Self-assembled nanostructured particle formed by evaporation-induced self-assembly (EISA) in an aerosol process.[7] (f) Plan view of a cubic mesoporous film[4] on a silicon substrate (satellite spots result from electron diffraction from the underlying silicon substrate). Images in (a) and (d) are courtesy of N. Liu, unpublished; (b) is from Reference 4.

essing) to create ordered nanostructured films, patterns, or particles (Figure 2).[4–7]

Understanding Self-Assembly

To understand EISA,[8] we have taken advantage of the steady-state nature of dip-coating. When a substrate is withdrawn vertically from a solution reservoir at a constant rate, a balance of upward moving liquid flux and evaporation causes the film thickness profile to become steady in the lab frame. This allows the complete EISA process (from the disordered dilute state near the reservoir surface to the highly ordered dry state) to be spatially resolved in the coating direction (normal to the reservoir surface).[9,10]

Figure 3 shows an optical interference image of a self-assembling silica/surfactant/ethanol/water system during dip-coating. Above the gravitational meniscus, where there is no longer any downward motion of the entrained liquid, the film thins exclusively due to evaporation, allowing us to calculate the evolving concentration of the nonvolatile silica and surfactant components (Figure 3b).

Using spatially resolved grazing incidence small-angle x-ray scattering (GISAXS, see Figures 4a–4d), we interrogate the periodic nanometer-scale structure as a function of thickness/composition, ultimately allowing the mapping of structure onto the appropriate ethanol/water/surfactant phase diagram (Figure 4). We find that the structure forms by an interfacially mediated process where, above the critical micelle concentration, oriented intermediate lamellar and correlated micellar structures (Figures 4b and 4c) form in compositional regions that are expected (on the basis of the ethanol/water/surfactant phase diagram, Figure 4a) to be isotropic. We attribute these discrepancies to the presence of interfaces and the introduction of silica, which serves as a second hydrophilic component. Enhanced solvent evaporation at the liquid/vapor interface promotes self-assembly there to form incipient lamellar silica/surfactant mesostructures that, based on *d* spacing, largely exclude ethanol and water. Further evaporation results in a correlated structure composed of wormlike cylindrical micelles that organize and align at the solid and vapor interfaces in a proto-hexagonal arrangement. Finally, an oriented hexagonal mesophase forms (Figure 4d) with its cylinder axes oriented parallel to the substrate surface. The hexagonal mesophase appears to be nucleated at the solid/liquid and liquid/vapor interfaces and, based on x-ray reflectivity experiments,[11] grows inward toward the film interior through conversion of the correlated wormlike mesostructure (Figure 4e).

Perhaps surprisingly, GISAXS studies on evaporating surfactant/water/ethanol systems prepared with and without oligosilicic acids as secondary hydrophilic components showed that silicic acid promoted the formation of ordered mesophases. This is explained by the silicic acid oligomers serving as *nonvolatile* hydrophilic components. By maintaining fluidity, they avoid kinetic barriers to self-assembly, as experienced in the silica-free system. Concerning thermodynamic factors, we found that by considering silicic acid to be equivalent (on a per mole silicon basis) to water, the first appearance of the hexagonal mesophase upon evaporation occurred near the isotropic/hexagonal phase boundary of the corresponding surfactant/water/ethanol system. This suggests that under acidic conditions, the oligosilicic acids have similar interactions with the hydrophilic head groups as water. To date, the appropriate quaternary silicic acid/water/ethanol/surfactant phase diagrams have not been determined experimentally.

Nanocomposite Self-Assembly

Self-assembly of silica/surfactant mesophases is normally followed by calcination or solvent extraction to remove the surfactant, creating a mesoporous material. Alternatively, we can use EISA to create *nanocomposite* materials in which organic polymers or other organic components are uniformly incorporated within a periodic inorganic nanostructure. The nanoscale organization of hard and soft materials is of interest for the development of optimized mechanical properties similar to those that occur in natural materials such as seashells, which are composed of alternating layers of crystalline calcium carbonate and biopolymers.

By using alcohol or tetrahydrofuran (THF) as a cosolvent, homogeneous, complex, multicomponent solutions can be prepared containing (in addition to the silicic acid precursors), organic monomers, cross-linkers, initiators, and coupling agents. During EISA, preferential evaporation of alcohol or THF concentrates the system in water. Rather than undergoing macroscopic phase separation, the hydrophobic components are incorporated into micelles and mesophases. As shown in Figure 5, this allows hundreds of alternating silica/organic layers to be organized in a single step.[12] Subsequent *in situ* organic/inorganic polymerization results in a poly(alkyl methacrylate)/silica nanocomposite with a covalently bonded polymer/silica interface. Such structures bear some relationship to seashells and other natural materials that are simultaneously hard, tough, and strong.

An alternative nanocomposite self-assembly strategy is to employ *polymerizable surfactants* as structure-directing agents and monomers.[13,14] The surfactant organizes the silicate nanostructure, as described earlier; then, light, heat, or another treatment is used to polymerize the surfactant

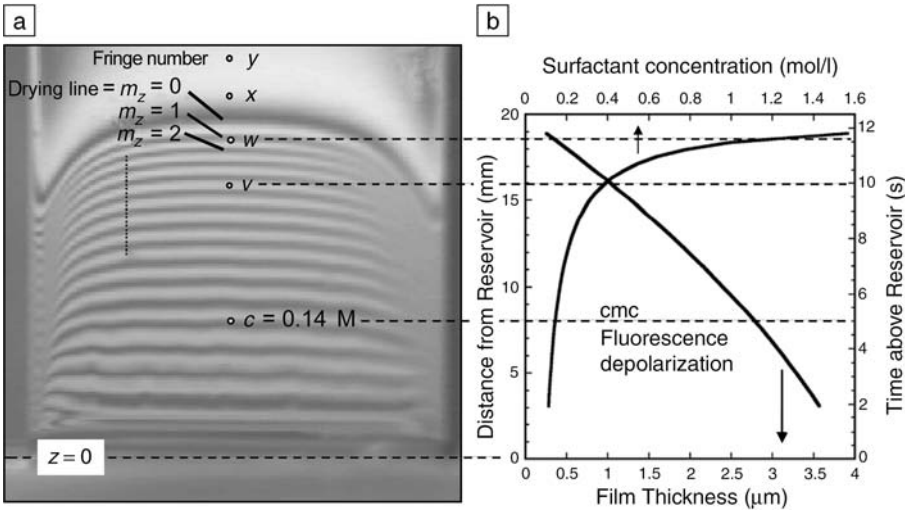

Figure 3. (a) Optical interference image of a steady-state film-drying profile used to calculate the film profile[10] (points y, x, w, v, *and* c *represent positions where spatially resolved grazing incidence small-angle x-ray scattering experiments were performed;* c *also represents the position of the critical micelle concentration. (b) Calculated film thickness and surfactant concentration corresponding to the interference image in (a). (Published with permission from the American Chemical Society).[10]*

monomers, uniformly confined within a nanometer-scale "reaction vessel." An advantage of this approach is that we expect the monomers to be uniformly organized within the surfactant mesophase, allowing potentially facile topochemical polymerization, where the topography of the monomeric diacetylenic (DA) assembly is preserved in the polymerized product, polydiactelyene.

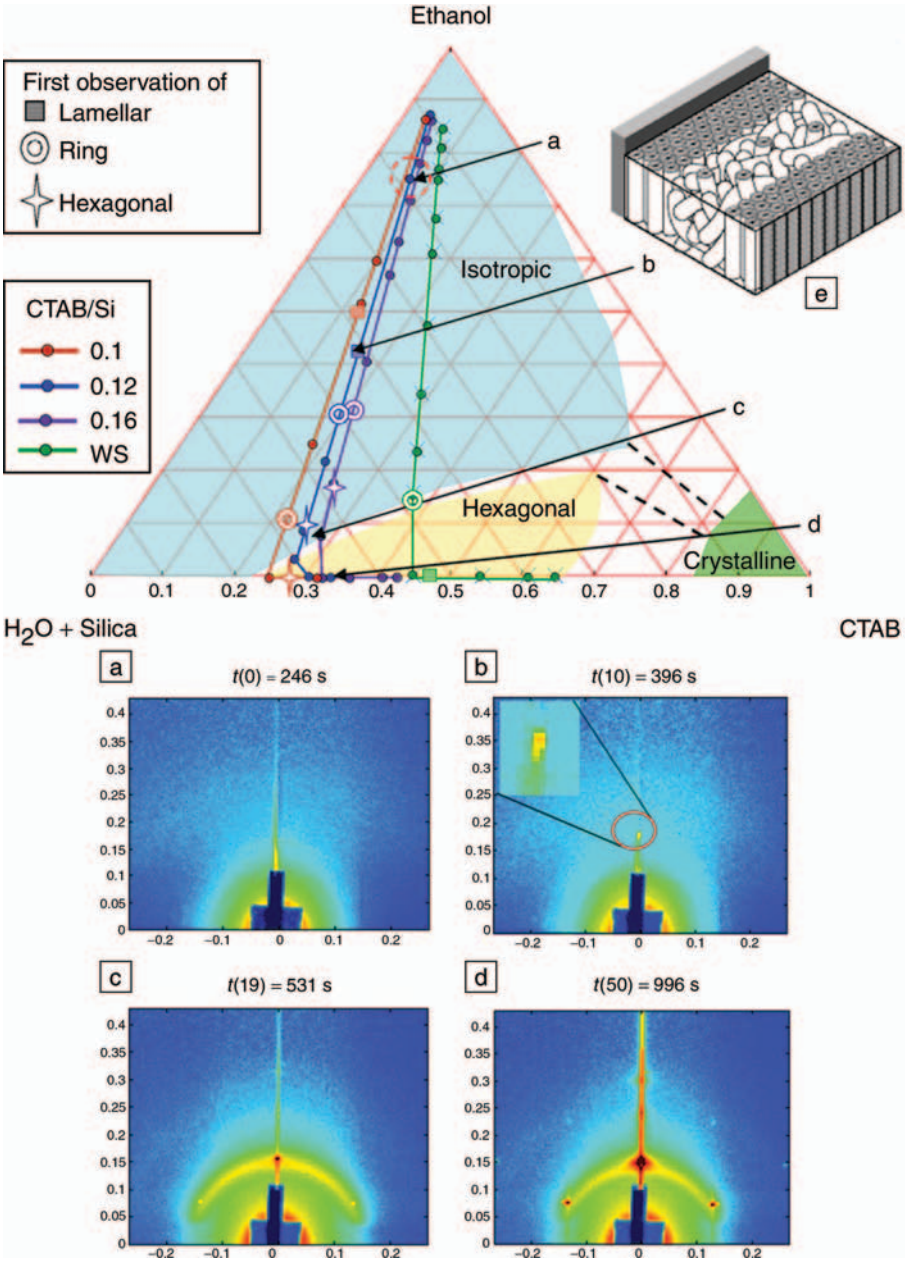

Figure 4. Bulk ternary H_2O/ethanol/surfactant phase diagram. The evaporation-induced compositional trajectories of the three cetyltrimethylammonium bromide (CTAB)/silica systems (0.10, 0.12, and 0.16, denoting the respective CTAB/silica molar ratios) and the WS (without silica) system (a solution prepared like sample 0.12, but without silica) are mapped onto the bulk water/ethanol/CTAB phase diagram, considering the hydrophilic silicic acid precursors to be equivalent to water. Grazing incidence small-angle x-ray scattering patterns obtained after a specified time t *(in seconds) are presented for sample 0.12, corresponding to the following: (a) the isotropic phase, (b) the lamellar mesophase, (c) the correlated micellar mesophase, and (d) the hexagonal mesophase; (e) ordered mesophase nucleates at liquid–vapor and solid–liquid interfaces and grows inward by conversion of the wormlike micellar interior. (Adapted from Reference 9.)*

In the example shown in Figure 6, DA surfactant monomers were prepared with hydrophilic oligoethylene oxide (EO) head groups. Increasing the number n of EO units comprising the head group progressively decreased the surfactant critical packing parameter g,[15,16] allowing the formation of lamellar, hexagonal, and cubic mesophases. UV exposure resulted in the formation of a blue polydiacetylene (PDA)/silica nanocomposite that exhibited thermo-, solvato- and mechanochromism, which are coloration effects occurring in response to thermal, mechanical, and chemical stimuli, respectively, to form the red fluorescent form (Figure 6d). A critical issue in this approach (and in self-assembly approaches in general) is the influence that nanoscale confinement has on polymerization and the structure/properties of the resulting product (e.g., organic polymers or silica). In this regard, it is noteworthy that the diacetylenic surfactants used to define the nanostructures shown in Figure 6 did not polymerize when assembled as a Langmuir monolayer on a flat surface. This implies that the curvature created by self-assembly (and then maintained by the self-assembled structure during polymerization) strongly influences the proximity/orientation of the reactive units and consequently their ability to polymerize. Perhaps more important, we anticipate that the polymer properties resulting from nano-confined polymerization will be different from those of their bulk counterparts. Understanding structural differences of such nano-confined materials and exploiting these differences to develop new functionalities represents an important and challenging future direction.

For example, in the case of polydiacetylene, we found that the PDA/silica nanocomposite exhibited reversible thermo- and mechanochromism, properties not normally observed in bulk PDA. For conjugated polymers in general, nanostructuring should allow much greater control of orientation and charge and energy transfer than for bulk materials. Also, the composite nanostructure should increase the chemical, thermal, and mechanical robustness of conjugated polymers, fostering their integration into devices.

Nanocrystal Self-Assembly

We can expand upon this composite self-assembly strategy by employing other hydrophobic components in addition to hydrophobic organic monomers/molecules. Recently, we investigated the self-assembly of hydrophobic nanocrystal (NC) mesophases within hydrophilic silica mesophases.[17] Most nanocrystal synthesis

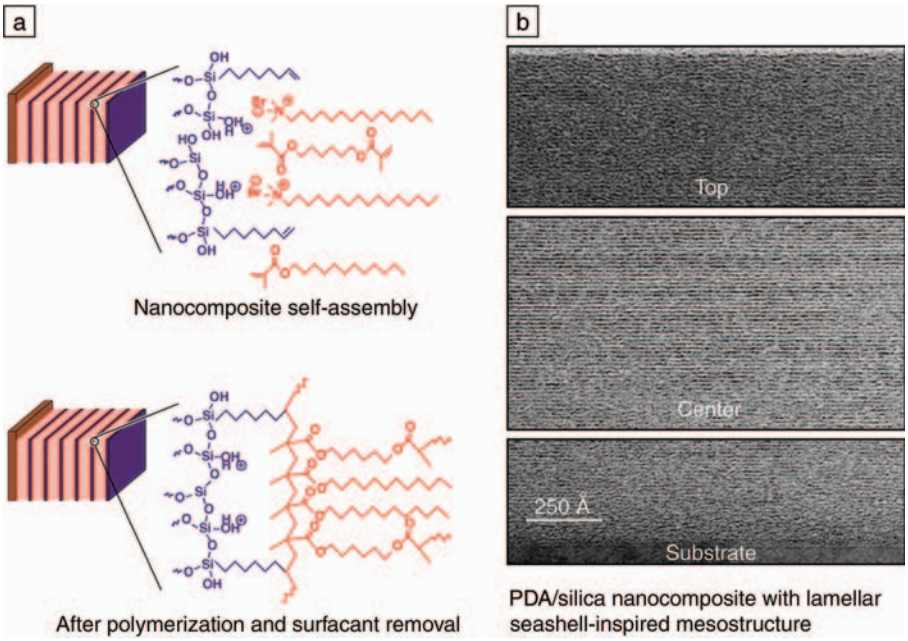

Figure 5. Evolution of nanolaminate structure during dip coating. (a), top schematic: Continued evaporation simultaneously organizes the inorganic and organic constituents into periodic thin-film mesophases. (a), bottom schematic: Combined organic/inorganic polymerization locks in the nanocomposite architecture. (b) Transmission electron microscopy images of a poly(alkyl methacrylate)/silica nanolaminate. (Adapted from Reference 12).

procedures use hydrophobic ligands (alkane thiols, trioctylphosphine oxide, etc.) to stabilize them from aggregation. Mono-sized NCs can be considered as moderate-sized hydrophobic molecules. We postulated that their incorporation as individual NCs in surfactant micelles would allow further self-assembly into ordered nanocrystalline mesophases, as anticipated from Figure 1. Rather than add hydrophobic NCs directly to isotropic surfactant/solvent/silica systems, as in polymer/silica self-assembly, a generic microemulsion procedure was developed to create water-soluble nanocrystal micelles. As represented schematically in Figure 7a, a concentrated nanocrystal solution prepared in organic solvent (chloroform, hexane, etc.), is added to an aqueous solution of surfactant under vigorous stirring to create an oil-in-water microemulsion. Organic solvent evaporation then transfers the NCs into the aqueous phase by an interfacial process driven by the hydrophobic van der Waals interactions between the primary alkanes of the NC stabilizing ligands and the secondary alkane of the surfactant. This results in thermodynamically defined interdigitated bilayer structures (Figure 7b). Cationic, anionic, and non-ionic surfactants and phospholipids can all form NC micelles, allowing facile control of micelle surface charge and functionality. In addition, fluorescent semiconducting CdSe NCs (stabilized by trioctylphosphine oxide) have been formed into NC micelles with maintenance of optical properties. This demonstrates the general nature and flexibility of this approach.

We discovered that in aqueous media, NC micelles organize hydrophilic components or precursors at the surfactant/water interface. This occurs through electrostatic and hydrogen-bonding interactions in a mechanism analogous to that of surfactant-directed self-assembly of silica/surfactant mesophases.[18] For example, addition of tetraethyl orthosilicate under basic conditions results in the formation of hydrophilic oligo-silicic acid species that organize with NC micelles to form a new type of ordered gold NC/silica mesophase. This nanocrystal mesophase has fcc symmetry (space group $Fm3m$), as shown in Figures 8a and 8b. These images are consistent with an fcc unit cell with dimension a of ~10.2 nm and uniform spacing between NCs of ~6 nm. Our work[17] appears to be the first example of an ordered fcc nanocrystal array formed spontaneously by self-assembly in aqueous media rather than by solvent evaporation.[19–21] Compared with other ordered NC arrays, the embedding silica matrix provides for greater chemical, mechanical, and thermal robustness. Furthermore, thermodynamically controlled self-assembly provides greater order and control of NC spacing, as compared with other connected nanocrystal systems such as those prepared by DNA hybridization.[22,23]

Using acidic conditions designed to minimize the siloxane condensation rate allows the formation of thin films by means of standard techniques like spin-coating, micromolding, or inkjet printing. By suppressing siloxane condensation, and thereby gel formation, solvent evaporation accompanying coating induces self-assembly of NC micelles into fcc nanocrystal thin-film mesophases. This occurs in a manner similar to the evaporation-induced self-assembly of cubic or hexagonal silica/surfactant thin-film mesophases discussed earlier.[4]

The metallic NC mesophases we describe appear to be the first examples [17]of highly ordered, fully three-dimensional (3D) nanocrystal arrays. NC arrays have been the subject of considerable interest, as they serve as model "artificial solids" with tunable electronic, magnetic, and optical properties stemming from single-electron charging and quantum confinement energies of individual NCs mediated by coupling interactions with neighboring NCs.

As an initial investigation of charge transport in an ordered 3D nanocrystal array, we fabricated planar metal–insulator–metal (MIM) devices, incorporating a Au NC/silica array as the insulator layer (see schematic inset in Figure 9a). We then measured their temperature-dependent I–V characteristics. The I–V curves for the gold NC/silica capacitors are plotted in Figure 9a. At room temperature, the I–V behavior is linear, with a zero-biased resistance of 14 MΩ, corresponding to a film resistivity of about 3×10^6 Ω cm. Nonlinearity near zero bias is evident at 200 K and increases with decreasing temperature. At 100 K and below, conduction occurs through the gold NC/silica insulator only above a minimum threshold voltage V_T, indicative of a collective Coulomb blockade[24] resulting from electrical isolation of the NCs. For such arrays of Coulomb islands, theory predicts that for $V > V_T$, current scales as a power law, $I = I_0(V/V_T - 1)^\zeta$. The scaling exponent ζ reflects the dimensionality of the accessible current-conducting pathways; for one and two dimensions, both modeling[25] and experiment[26] show ζ to approximately equal the array dimensionality. Figure 9b plots representative I–V scaling data for our 3D gold NC/silica arrays measured at 78 K. We observe power-law scaling with $\zeta = 2.7$ (negative bias) and $\zeta = 3.1$ (positive bias). Note that bias here refers to the sign of the voltage in the current–voltage

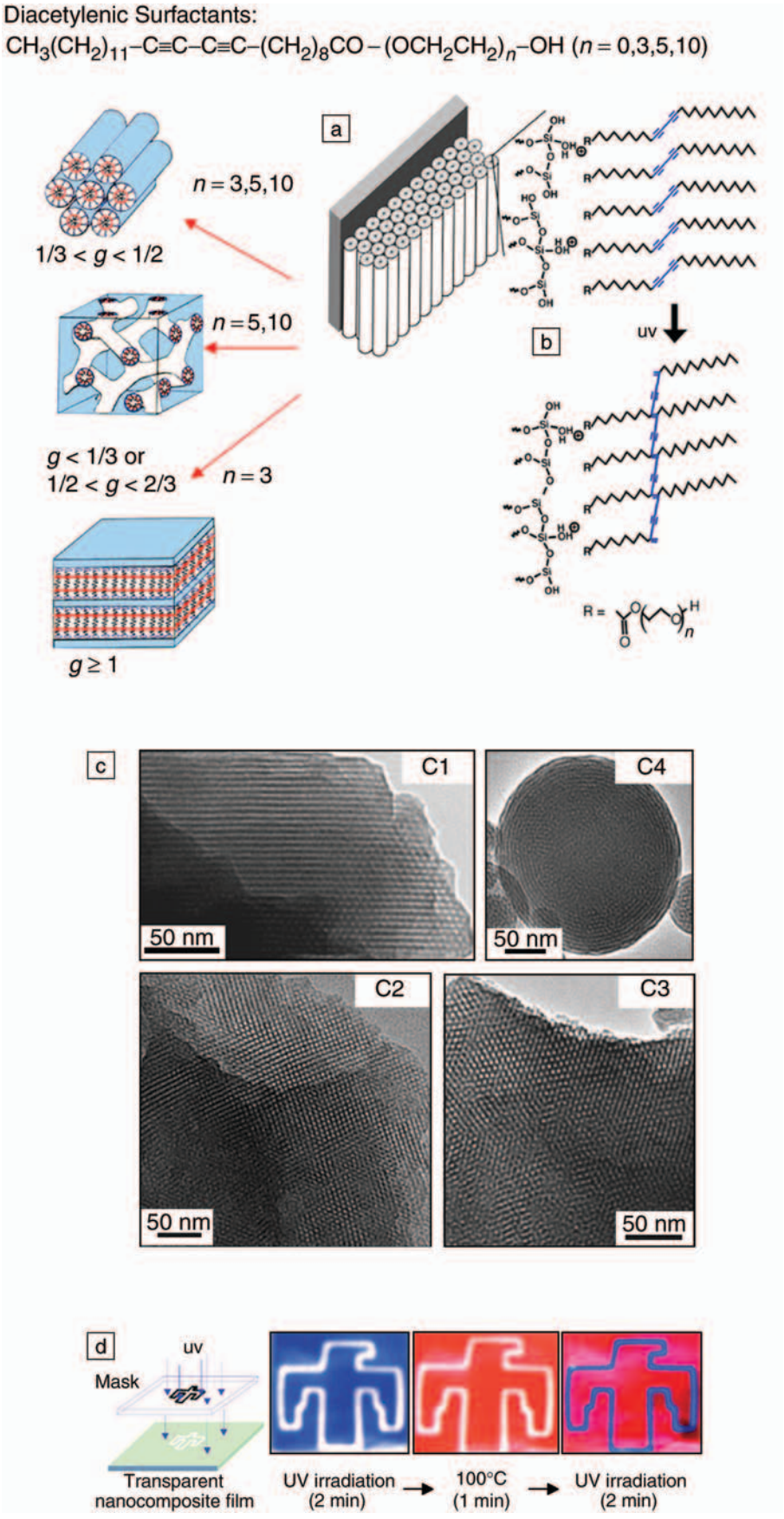

Figure 6. (a) Molecular structures of diacetylenic (DA) surfactants and polymerization of DA/silica nanocomposites. (b) DA surfactants serve both as amphiphiles to direct the self-assembly of the silicic acid mesostructure and as monomeric precursors of the conjugated polymer, polydiacetylene (PDA). Increasing the number n *of oligoethylene oxide (EO) subunits comprising the hydrophilic surfactant head group results in the formation of higher-curvature mesophases: lamellar (*n = *3) → hexagonal (*n = *5) → cubic (*n = *10), due to a decreasing value of the surfactant packing parameter* g*. (c) Representative transmission electron microscopy images of nanocomposite thin films and particles. C1: [110]-oriented hexagonally ordered nanocomposite film prepared using 2.23% DA-EO_5. C2 and C3: Two orientations ([100] and [111]) of a cubic nanocomposite film. C4: PDA/silica nanocomposite particles prepared using an aerosol-assisted evaporation-induced self-assembly technique. (d) Patterned polymerization induced by UV irradiation and thermochromic transition of hexagonal PDA/silica nanocomposite films. (Adapted from Reference 13).*

plot in Figure 9a. Currently, there are no theoretical predictions or simulations of the 3D scaling exponent; however, the greater value of ζ observed here, compared with previous studies of 2D arrays[26] and quasi-3D arrays,[27] is consistent with the greater number of conductive pathways expected for a fully 3D array.

In general, such highly ordered NC arrays should serve as model ideal systems in which to discover new nanoscale phenomena and to develop and test theories of collective optical, electronic, and magnetic behaviors.

Responsive Systems

Living systems are able to sense and respond to their environments through various chemical- and physical-based transduction mechanisms. From an engineering perspective, robust materials that respond predictably to pH,[28–31] temperature,[31,32] light,[33–38] biomolecules,[39–41] or electric fields[42,43] could find applications in controlled release of drugs or corrosion inhibitors, sensors, optical storage, and optomechanical actuation. So the question arises, how do we impart responsive, lifelike qualities to robust engineering materials?

In examining biological systems, we note that responsiveness often derives from hierarchical assemblies that position environmentally sensitive moieties onto a 3D framework. In an attempt to emulate such

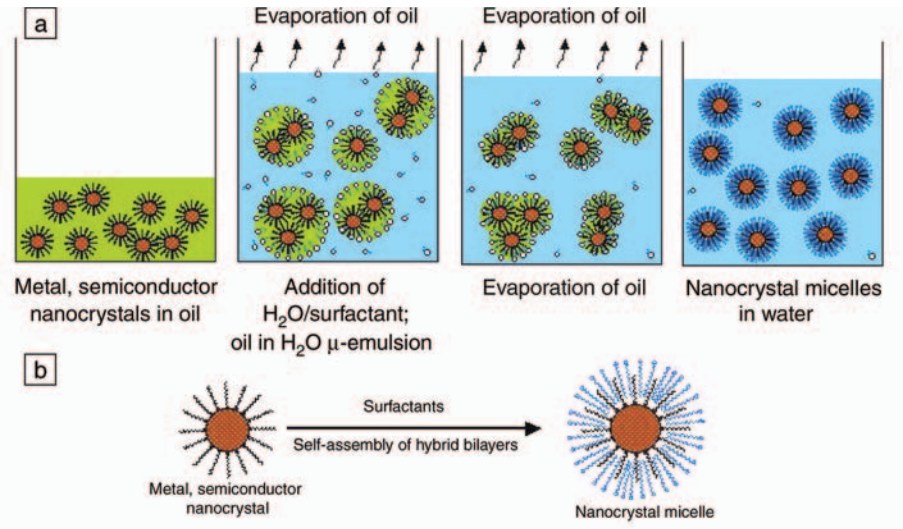

Figure 7. (a) Process scheme for the synthesis of water-soluble nanocrystal micelles. The addition of oil containing gold nanocrystals (NCs) to a surfactant containing aqueous solution during vigorous stirring leads to the formation of an oil in H_2O microemulsion. Subsequent evaporation of oil transfers the NCs into the aqueous phase by an interfacial process driven by the hydrophobic van der Waals interactions between the primary alkane of the stabilizing ligand and the secondary alkane of the surfactant, resulting in thermodynamically defined interdigitated bilayer structures that encapsulate the NCs and make them water-soluble (b).

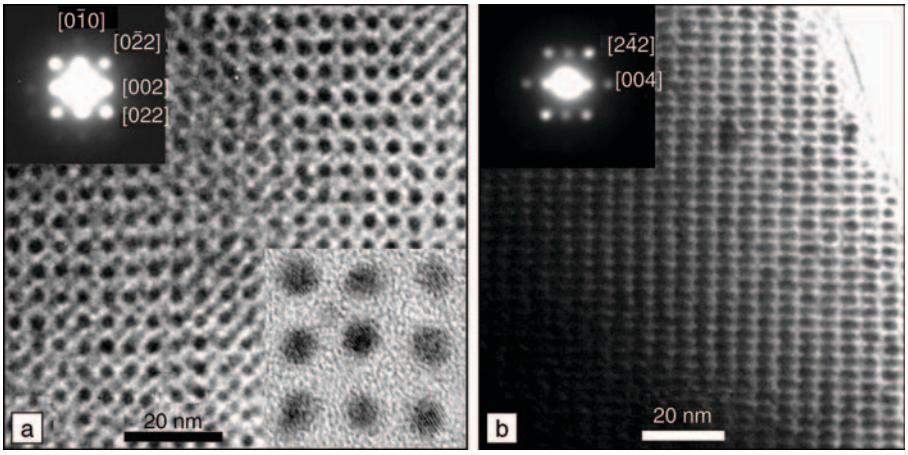

Figure 8. Representative transmission electron microscopy (TEM) images of Au nanocrystal/silica mesophases. (a) [100] and (b) [210] orientations of bulk samples. Lower-right inset in (a): High-resolution TEM of sample in (a) showing gold NC lattice fringes. Upper-left inset in (a): Selected-area diffraction (SAED) pattern from the image in (a). Inset in (b): SAED pattern from the image in (b). (Adapted from Reference 17.)

biological designs, our idea was to organize optically[33–35] and thermally[31] responsive azobenzene molecules within a robust, ordered 3D nanostructure using self-assembly (see Figure 10). In this synergistic design, photo or thermal energy is transduced into a 3D mechanical response that can control pore size and transport behavior.

Azobenzene derivatives were selected because of their well-studied response to light.[44–47] *Trans* ↔ *cis* isomerization changes the molecular dimension (molecular length of the *cis* isomer is ~3.4 Å shorter than that of the *trans* isomer) and also the dipole moment (0.5–3.1 D). Azobenzenes have been used previously to achieve switchable properties. However, in order to accurately control pore size, we needed to anchor azobenzene ligands to the pore surfaces of a nanostructured scaffold composed of mono-sized pores. This allows the rigid inorganic scaffold to precisely position azobenzene ligands in 3D configurations, where switching results in a well-defined change in pore size (see Figure 11). The 3D composite architecture should also enhance mechanical and thermal stability of the switchable ligands, important for their integration into devices.

Our synthesis[33–35] scheme employed an azobenzene-modified silane, 4-(3-triethoxysilylpropylureido)azobenzene (TSUA), designed to serve as an amphiphilic cosurfactant after hydrolysis of the ethoxy groups. During EISA, the hydrophobic propylureidoazobenzene groups are positioned in the hydrophobic micellar cores. The hydrophilic head groups co-organize with added silicic acid oligomers at the hydrophilic micellar exteriors. After catalytic or thermally promoted siloxane condensation, azobenzene ligands are anchored to the surfaces of mono-sized pores, with the azobenzene ligands oriented toward the pore interiors (see Figure 11). Subsequent surfactant extraction produces the target nanocomposite.

Figure 12 shows a transmission electron microscopy (TEM) cross-sectional image of an as-prepared photoresponsive nanocomposite film that exhibits a highly ordered cubic mesostructure. The average center-to-center pore spacing is 5.6 nm. Two-dimensional GISAXS data confirm that the pores are arranged in a (100)-oriented bcc mesostructure ($Im\bar{3}m$ space group), with $a = 5.7$ nm.

As determined with UV–visible spectroscopy, UV irradiation of the *trans* isomer causes transformation to the *cis* isomer. Removal of the UV radiation, irradiation with a longer wavelength, or heating switches the system back to the *trans* form. As a control experiment, we made films with the same sol but prepared without the non-ionic Brij56 surfactant. In this case, the azobenzene ligands were randomly incorporated in a microporous silica matrix (pore diameter, less than 1 nm) and exhibited no detectable photoisomerization. Similarly, we observed no photoisomerization for the ordered self-assembled films prior to solvent extraction of the surfactant templates. Only upon surfactant removal did we create the pore volume required (estimated as 127 Å^3)[48] for photoisomerization. These results unambiguously locate the photosensitive azobenzene ligands along with surfactant within the uniform nanopores of the self-assembled films. They emphasize the need to accommodate the steric demands of the photoisomerization process by engineering the pore size and positioning the photoactive species on the pore surfaces.

To demonstrate optical control of mass transport, we performed a chronoamperometry experiment using an azobenzene-

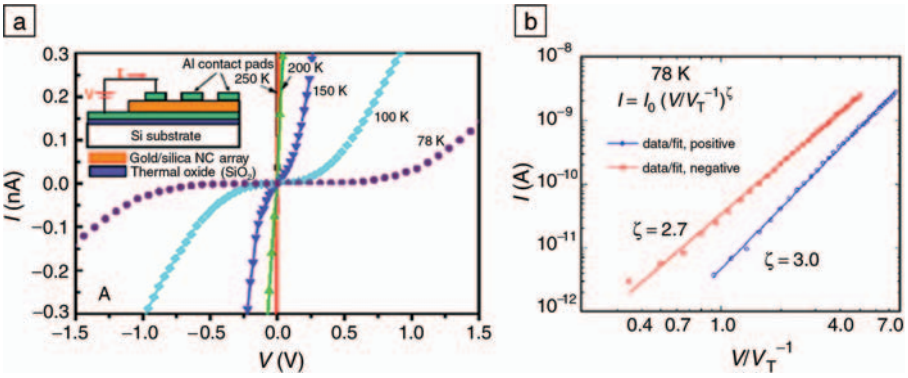

Figure 9. (a) Current–voltage (I–V) curves measured from 300 K to 78 K. The schematic in (a) shows the architecture of a metal–insulator–metal (MIM) device, fabricated with a 100-nm-thick Au/silica nanocrystal array as the insulator. (b) At T = 78 K, current displays a power-law dependence for $V > V_T$, with scaling exponent $\zeta = 2.7$ (negative bias) and $\zeta = 3.0$ (positive bias). V_T and ζ were determined by the Levenberg–Marquardt nonlinear least-squares method. (Adapted from Reference 17.)

functionalized nanocomposite membrane to modify the working electrode in an electrochemical cell (see Figure 13). The chronoamperometry experiment uses ferrocene dimethanol (FDM) as a molecular probe and provides a measure of mass transport through the nanocomposite membrane by monitoring the steady-state oxidative current at constant potential for the reaction taking place on the working electrode surface, which is indium tin oxide (ITO). At constant potential, the effective pore size limits the diffusion rate of probing molecules to the electrode surface during electrolysis. Under dark conditions, the azobenzene moieties are predominantly in their extended *trans* form. Upon UV irradiation ($\lambda = 360$ nm), the azobenzene moieties isomerize to the more compact *cis* form, which we expected would increase the diffusion rate and, correspondingly, the oxidative current. Likewise, exposure to visible light ($\lambda = 435$ nm) triggers the reverse *cis* → *trans* isomerization of the azobenzene moieties, which should decrease the current to the pre-UV exposure level.

Figure 14 shows typical current versus time photoresponse data for the membrane-modified electrode. We observe that after an initial transient decay, the oxidative current of ferrocene dimethanol reaches a steady state after about 360 s. Upon UV irradiation, the current increases progressively due to *trans* → *cis* isomerization, which increases the pore size. It then reaches a new plateau, corresponding to the photostationary state of *trans* → *cis* isomerization. Visible-light exposure decreases the oxidative current due to *cis* → *trans* isomerization, which decreases the pore size. After 200 s, the current is reduced to its pre-UV exposure level. This corresponds to the photostationary state of *cis* → *trans* isomerization. We performed three cycles of alternating UV/visible light exposure to show the reversibility and repeatability of this process. In the last cycle, a much weaker visible light (0.5 mW) was used instead of the stronger visible light (5.6 mW). We observed a much slower decrease in current, demonstrating a slower response under lower illumination levels. Control experiments were performed on a bare ITO electrode and one coated with mesoporous silica. However, no photoresponse was observed in either of these systems. This demonstrates that the photoresponse is not an artifact of the ITO electrode or the mesoporous silica film, but a true effect arising from the isomerization

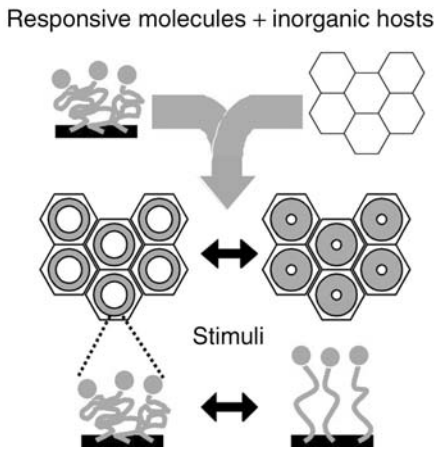

Figure 10. Concept of responsive nanocomposites. Organization of stimulus-responsive ligands within a three-dimensional porous framework imparts new molecular-level functionality, useful for opening and closing a nanoscale valve. (Adapted from Bruce Bunker, unpublished work.)

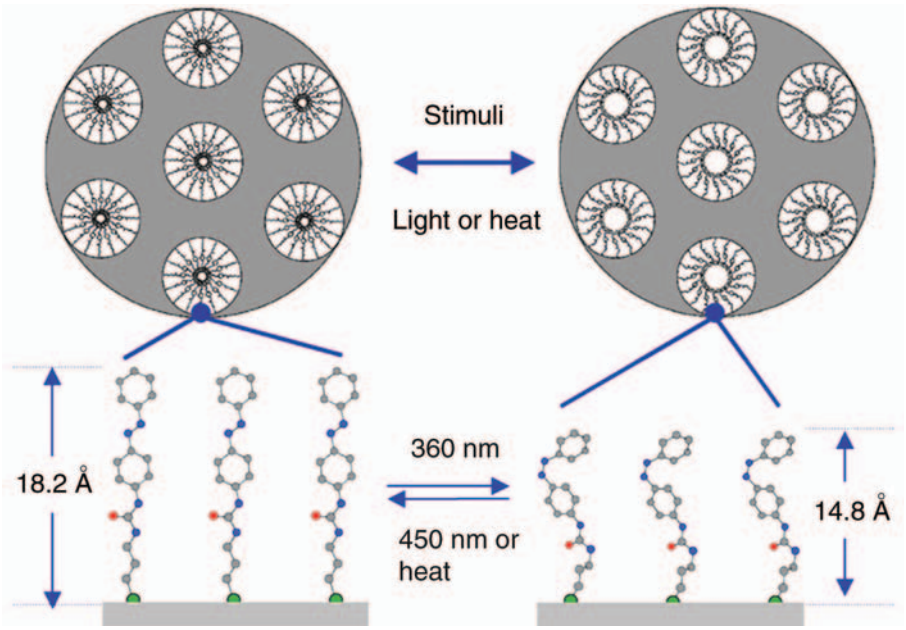

Figure 11. Schematic illustration of photoresponsive nanocomposites prepared by evaporation-induced self-assembly. The trans *or* cis *conformation of the azobenzene unit was calculated using Chem3D Pro molecular modeling analysis software. Atomic legend: grey, carbon; red, oxygen; blue, nitrogen; green, silicon; H atoms are omitted. (Adapted from Reference 33).*

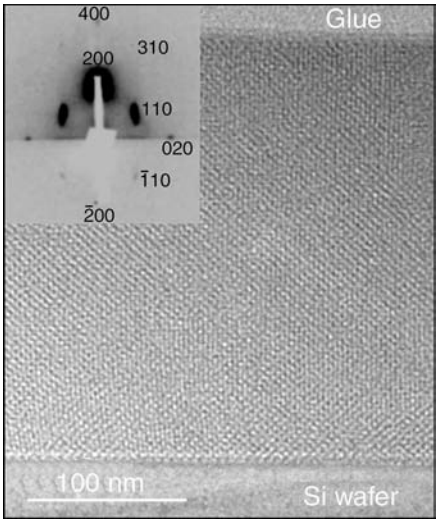

Figure 12. Cross-sectional transmission electron microscopy image of a photoresponsive nanoporous film.[34] Inset: Two-dimensional grazing incidence small-angle x-ray scattering pattern, shown in reverse gray scale. The lower half-plane is in the shadow of the silicon substrate, and the scattering spots are attenuated. (Published with permission of the American Chemical Society.)[34]

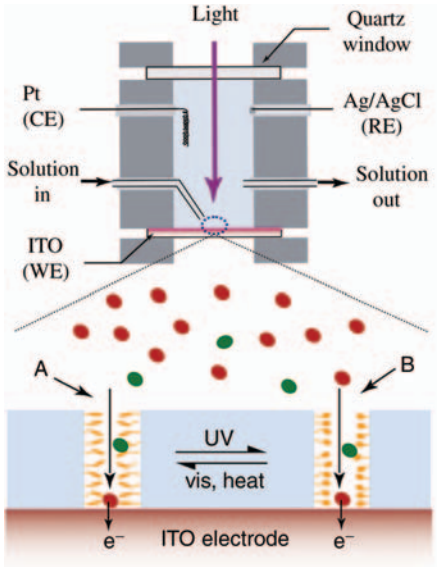

Figure 13. Schematic drawing of (top) an electrochemical cell and (bottom) mass transport of probing molecules through the photoresponsive nanocomposite membrane integrated on an indium tin oxide (ITO) electrode.[34] A: Diffusion through smaller pores with azobenzene ligands in their trans *configuration. B: Diffusion through larger pores with azobenzene ligands in their* cis *configuration. Red ovals are FDM (ferrocene dimethanol); green ovals are FDM^{++}; small orange ovals are azobenzene in* cis *form; small elongated orange ovals are azobenzene in* trans *form. CE, RE, and WE refer to the counter electrode, reference electrode, and working electrode, respectively. (Published with permission from the American Chemical Society.)[34]*

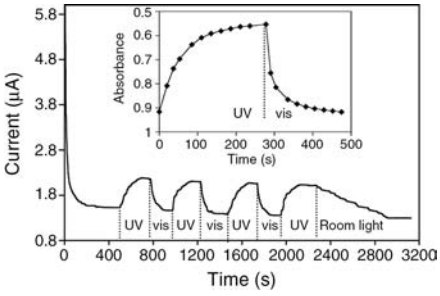

*Figure 14. Current–time (*I–t*) behavior of a photoresponsive nanocomposite film under alternate exposure to UV (360 nm) and visible light (435 nm). Last cycle uses room light, 400–700 nm. Inset shows absorbance at 356 nm ($\pi-\pi^*$ transition of the* trans *isomer) of the same film immersed in a buffer solution containing 1 mM FDM (ferrocene dimethanol). The time scale of the UV/vis data corresponds to that of the first cycle in the* I–t *response curve using FDM as the molecular probe. (Adapted from Reference 34.)*

of azobenzene moieties attached to the nanopore surfaces.

To correlate the observed current changes with the actual isomerization state, a UV/visible spectroscopy study was performed, where the nanocomposite film used for chronoamperometry was immersed in the electrolyte solution and illuminated exactly as for the first *I–t* cycle in the chronoamperometry experiment. As shown in the inset of Figure 14, the absorbance of the nanocomposite film at 356 nm, attributed to the $\pi-\pi^*$ transition of azobenzene in the *trans* form, decreases progressively under UV irradiation, reaching a plateau corresponding to the photostationary state of *trans* → *cis* isomerization. The following visible-light exposure causes the reverse *cis* → *trans* isomerization, increasing the absorbance gradually before reaching the pre-UV state. These data exactly correlate the conformational changes of azobenzene moieties in the nanocomposite film with the oxidative current changes measured in the chronoamperometry experiment. Thus, we clearly demonstrate control of mass transport on the nanoscale.

Conclusion

I hope I have convinced the reader of the power of self-assembly as a means to precisely organize complex (and often disparate) materials on the nanoscale. Our variations on the theme of evaporation-induced self-assembly allow nanostructures to be integrated easily into devices and, in some cases, provide a pathway to materials that have no bulk nanostructured counterparts (e.g., organic/inorganic nanocomposites). Many challenges remain, however. Our self-assembled nanostructures, although beautiful, are boringly repetitive. To better emulate biology, we need to break symmetry and develop structure and function on a broader range of length scales. I expect there to be much future progress in so-called directed assembly, where active intervention such as the application of an external field can be used to perturb or modulate the assembly process. Currently, there is much interest in structure formation by energy-dissipating systems, where large-scale patterns often emerge. Combined with smaller-scale molecular self-assembly, this may be a means of developing hierarchical structures. Finally, we should consider compartmentalized synthesis, for example, within membrane-bound molds, where selective ion channels are used to spatially control pH, ionic strength, and the introduction of precursor ions. Such an approach could allow the formation of synthetic analogues to natural structures like diatoms and spicules.

Acknowledgments

This work has benefited tremendously from the research of creative students and postdoctoral fellows including Yunfeng Lu, Hongyou Fan, Dhaval Doshi, Bernd Smarsly, Ralf Koehn, Yi Yang, Nanguo Liu, and Alan Sellinger. I also have profited from collaborations with my colleagues at Sandia and the University of New Mexico, including Alan Hurd (now at Los Alamos), Frank van Swol, Kevin Malloy, Darren Dunphy, Darryl Sasaki, Alain Burns, Gabriel Lopez, and Abhaya Datye, and visiting professor Alain Gibaud (Université du Maine, Le Mans, France). This work was partially supported by the U.S. Department of Energy Basic Energy Sciences Program, the Air Force Office of Scientific Research, the National Science Foundation (NIRT, NNIN, and the Ceramic Composite Materials Center programs), the Army Research Office, Sandia National Laboratory's laboratory-directed R&D program and the Center for Integrated Nanotechnologies, and DARPA. TEM investigations were performed in the Department of Earth and Planetary Sciences at the University of New Mexico. Sandia is

a multiprogram laboratory operated by Sandia Corporation, a Lockheed Martin Company, for the U.S. Department of Energy's National Nuclear Security Administration under contract DE-AC04-94ALB5000.

References

1. G.M. Whitesides and B. Grzybowski, *Science* **295** (2002) p. 2418.
2. C. Kresge, M. Leonowicz, W. Roth, C. Vartuli, and J. Beck, *Nature* **359** (1992) p. 710.
3. C.J. Brinker and G.W. Scherer, *Sol-Gel Science: The Physics and Chemistry of Sol-Gel Processing* (Academic Press, San Diego, 1990).
4. Y. Lu, R. Ganguli, C. Drewien, M. Anderson, C. Brinker, W. Gong, Y. Guo, H. Soyez, B. Dunn, M. Huang, and J. Zink, *Nature* **389** (1997) p. 364.
5. H. Fan, Y. Lu, A. Stump, S. Reed, T. Baer, R. Schunk, V. Perez-Luna, G. Lopez, and C. Brinker, *Nature* **405** (2000) p. 56.
6. D. Doshi, N. Huesing, M. Lu, H. Fan, Y. Lu, K. Simmons-Potter, B. Potter, A. Hurd, and C. Brinker, *Science* **290** (2000) p. 107.
7. Y. Lu, H. Fan, A. Stump, T. Ward, T. Rieker, and C. Brinker, *Nature* **398** (1999) p. 223.
8. C. Brinker, Y. Lu, A. Sellinger, and H. Fan, *Adv. Mater.* **11** (1999) p. 579.
9. D. Doshi, A. Gibaud, V. Goletto, M. Lu, H. Gerung, B. Ocko, S. Han, C. Brinker, *J. Am. Chem. Soc.* **125** (2003) p. 11646.
10. D. Doshi, A. Gibaud, N. Liu, D. Sturmayr, A. Malanoski, D. Dunphy, H. Chen, S. Narayanan, A. MacPhee, J. Wang, S. Reed, A. Hurd, F. van Swol, and C. Brinker, *J. Phys. Chem. B* **107** (2003) p. 7683.
11. A. Gibaud, D. Grosso, B. Smarsly, A. Baptiste, J. Bardeau, F. Babonneau, D. Doshi, Z. Chen, C. Brinker, and C. Sanchez, *J. Phys. Chem. B* **107** (2003) p. 6114.
12. A. Sellinger, P. Weiss, A. Nguyen, Y. Lu, R. Assink, W. Gong, and C. Brinker, *Nature* **394** (1998) p. 256.
13. Y. Lu, Y. Yang, A. Sellinger, M. Lu, J. Huang, H. Fan, R. Haddad, G. Lopez, A. Burns, D. Sasaki, J. Shelnutt, and C. Brinker, *Nature* **410** (2001) p. 913.
14. Y. Yang, Y. Lu, M. Lu, J. Huang, R. Haddad, G. Xomeritakis, N. Liu, A. Malanoski, D. Sturmayr, H. Fan, D. Sasaki, R. Assink, J. Shelnutt, F. van Swol, G. Lopez, A. Burns, and C. Brinker, *J. Am. Chem. Soc.* **125** (2003) p. 1269.
15. J.N. Israelachvili, *Intermolecular and Surface Forces* (Academic Press, San Diego, 1992).
16. J.N. Israelachvili, D.J. Mitchell, and B.W. Ninham, *J. Chem. Soc.* **2** (1976) p. 1525.
17. H. Fan, K. Yang, D.M. Boye, T. Sigmon, K.J. Malloy, G.P. Lopez, C.J. Brinker, and H. Xu, *Science* **304** (2004) p. 567.
18. J.S. Beck, J.C. Vartuli, W.J. Roth, M.E. Leonowicz, C.T. Kresge, K.D. Schmitt, C.T.-W. Chu, D.H. Olson, E.W. Sheppard, S.B. McCullen, J.B. Higgins, and J.L. Schlenker, *J. Am. Chem. Soc.* **114** (1992) p. 10834.
19. C.B. Murray, C.R. Kagan, and M.G. Bawendi, *Science* **270** (1995) p. 1335.
20. S.H. Sun, C.B. Murray, D. Weller, L. Folks, and A. Moser, *Science* **287** (2000) p. 1989.
21. C.B. Murray, C.R. Kagan, and M.G. Bawendi, *Science* **270** (1995) p. 1335.
22. A.P. Alivisatos, K.P. Johnsson, X.G. Peng, T.E. Wilson, C.J. Loweth, M.P. Bruchez, and P.G. Schultz, *Nature* **382** (1996) p. 609.
23. C.A. Mirkin, R.L. Letsinger, R.C. Mucic, and J.J. Storhoff, *Nature* **382** (1996) p. 607.
24. H. Grabert and M.H. Devoret, *Single Charge Tunneling* (Plenum Publishers, New York, 1992).
25. A.A. Middleton and N.S. Winggreen, *Phys. Rev. Lett.* **71** (1993) p. 3198.
26. A.J. Rimberg, T.R. Ho, and J. Clarke, *Phys. Rev. Lett.* **74** (1995) p. 4714.
27. C.T. Black, C.B. Murray, R.L. Sandstrom, and S.H. Sun, *Science* **290** (2000) p. 1131.
28. D.J. Beebe, J.S. Moore, J.M. Bauer, Q. Yu, R.H. Liu, C. Devadoss, and B.-H. Jo, *Nature* **404** (2000) p. 588.
29. Q. Yu, J.M. Bauer, J.S. Moore, and D.J. Beebe, *Appl. Phys. Lett.* **78** (2001) p. 2589.
30. R.H. Liu, Q. Yu, and D.J. Beebe, *J. Microelectromech. Syst.* **11** (2002) p. 45.
31. G. Garnweitner, B. Smarsly, R. Assink, W. Ruland, E. Bond, and C.J. Brinker, *J. Am. Chem. Soc.* **125** (2003) p. 5626.
32. R. Yoshida, K. Uchida, Y. Kaneko, K. Sakai, A. Kikuchi, Y. Sakurai, and T. Okano, *Nature* **374** (1995) p. 240.
33. N. Liu, Z. Chen, D. Dunphy, Y. Jiang, R. Assink, and C. Brinker, *Angew. Chem., Int. Ed. Engl.* **42** (2003) p. 1731.
34. N. Liu, D.R. Dunphy, P. Atanassov, S.D. Bunge, Z. Chen, G.P. Lopez, T.J. Boyle, C.J. Brinker, *Nanolett.* **4** (2004) p. 551.
35. N. Liu, D.R. Dunphy, M.A. Rodriguez, S. Singer, C.J. Brinker, *Chem. Commun.*, (2003) p. 1144.
36. N.K. Mal, M. Fujiwara, and Y. Tanaka, *Nature* **421** (2003) p. 350.
37. H. Rau, in *Photochemistry and Photophysics*, Vol. II, edited by J. Rabek (CRC Press, Boca Raton, FL, 1990).
38. A. Natansohn, in *Macromolecular Symposia*, edited by H. Höcker, W. Guth, B. Jung, I. Meisel, and S. Spiegel (WILEY-VCH, Weinheim, Germany, 1999) p. 1.
39. K. Kataoka, H. Miyazaki, M. Bunya, T. Okano, and Y. Sakurai, *J. Am. Chem. Soc.* **120** (1998) p. 12694.
40. E. Kokufuta, Y.Q. Zhang, and T. Tanaka, *Nature* **351** (1991) p. 302.
41. T. Miyata, N. Asami, and T. Uragami, *Nature* **399** (1999) p. 766.
42. T. Tanaka, I. Nishio, S.T. Sun, and S. Uenonishio, *Science* **218** (1982) p. 467.
43. I.C. Kwon, Y.H. Bae, and S.W. Kim, *Nature* **354** (1991) p. 291.
44. G.S. Kumar and D.C. Neckers, *Chem. Rev.* **89** (1989) p. 1915.
45. M. Ueda, H.-B. Kim, T. Ikeda, and K. Ichimura, *Chem. Mater.* **4** (1992) p. 1229.
46. L.M. Siewierski, W.J. Brittain, S. Petrash, and M.D. Foster, *Langmuir* **12** (1996) p. 5838.
47. M. Ogawa, K. Kurodacd, and J.-I. Moric, *Chem. Commun.* (24) (2000) p. 2441.
48. J.G. Victor and J.M. Torkelson, *Macromolecules* **20** (1987) p. 2241. □

C. Jeffrey Brinker *received his BS, MS, and PhD degrees in ceramic science and engineering at Rutgers University. He joined Sandia National Laboratories (SNL) as a member of the technical staff in 1979. He was promoted to Distinguished Member of the Technical Staff at SNL and appointed Distinguished National Laboratory Professor of Chemistry and Chemical Engineering at the University of New Mexico (UNM) in 1991. Since 1999, he has been jointly employed at SNL, where he is a Sandia Fellow, and at UNM, where he is a professor of Chemical and Nuclear Engineering and co-director of the Center for Micro-Engineered Materials.*

Several of Brinker's 250-plus publications are among the highest cited in materials research. Among Brinker's most recent honors are election to the National Academy of Engineering (2002) and recipient of the Department of Energy's Ernest O. Lawrence Memorial Award in Materials Science (2002).

Brinker can be reached by e-mail at cjbrink@sandia.gov.